Reaction of Benzene Molecule on Size-Selected Nickel Cluster Ions

Tetsu Hanmura,[†] Masahiko Ichihashi,[‡] and Tamotsu Kondow*[,‡]

East Tokyo Laboratory, Genesis Research Institute, Inc., 717-86 Futamata, Ichikawa, Chiba 272-0001, Japan, and Cluster Research Laboratory, Toyota Technological Institute, in East Tokyo Laboratory, Genesis Research Institute, Inc., 717-86 Futamata, Ichikawa, Chiba 272-0001, Japan

Received: November 14, 2001; In Final Form: February 28, 2002

Absolute cross sections for the reaction of a benzene molecule with a nickel cluster cation with the sizes of 3−11 were measured in a beam-gas cell geometry at collision energies less than 1 eV in a tandem mass spectrometer. Three different reaction processes were found to proceed: benzene chemisorption with and without Ni release and dissociative chemisorption with C_2H_2 release. The size-dependent reaction cross sections were explained in terms of a statistical model.

1. Introduction

The reactivity of nickel clusters changes with their sizes (number of the constituent atoms) dramatically. For instance, hydrogenation of benzene on nickel aggregates with the sizes of several thousands proceeds favorably.[1] More favorable sizes for the hydrogenation could be observed in smaller sizes, on the basis of the fact that a reactant molecule on a metal surface interacts with the surface metal atoms in the close vicinity of the molecule.[2] In this connection, several groups have so far investigated reactions of nickel clusters ions, Ni_n^+, with simple molecules in the gas phase under multiple collision.[3−9] For instance, Wöste and co-workers have observed adsorption of CO on a size-selected nickel cluster ion with the sizes of 4−31 in a drift tube.[3,4] They have shown that nickel cluster ions with the sizes of 4−6 react with CO rapidly. Irion and co-workers have revealed that ethylene dehydrogenation takes place on nickel cluster ions with the sizes of 5 or above, while benzene is chemisorbed at the sizes of 3−4 and dissociatively chemisorbed at the sizes larger than 4.[5,6]

It is necessary to study such reactions under a single-collision condition in the case when the origin of the size dependence of the reactions is bound to be elucidated. To this end, we investigated reactions of a size-selected nickel cluster ion having the sizes of 3−11 with a benzene molecule in a condition that the cluster ion and the molecule collide only once. We found three reaction processes, and their absolute reaction cross sections were measured at different collision energies and cluster sizes, as well as at the cluster temperatures of 300 and 77 K. A statistical model was applied to analyze the results.

2. Experimental Section

The apparatus employed is described briefly in this report (see refs 9−12 for detailed description). Figure 1 shows a schematic diagram of the apparatus consisting of a cluster ion source, a cooling cell, two quadrupole mass spectrometers, a collision cell and an ion detector. Cluster ions were produced by sputtering of 10-keV xenon ions onto four water-cooled nickel targets (Nilaco, 99.7%) and were cooled in the first octopole ion guide filled with He gas of 10^{-3} Torr having the temperatures of 300 or 77 K. A size-selected cluster ion from the first quadrupole mass spectrometer was allowed to collide with a benzene molecule in the collision cell. Commercially available benzene (Kanto Chemical, >99.5%) was used without further purification. The pressure in the collision cell measured by a spinning rotor gauge was kept at 5×10^{-5} Torr, at which the single-collision condition is fulfilled. Product ions from the collision cell were mass-analyzed in the second quadrupole mass spectrometer and observed by a detector consisting of an ion-conversion dynode and a secondary electron multiplier. The signal from the detector was amplified, discriminated, and registered in a personal computer (NEC, PC-9801RA).

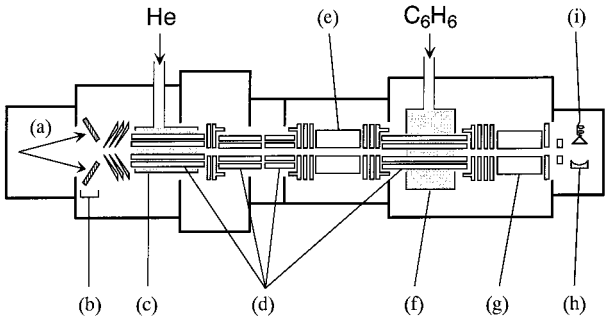

Figure 1. Schematic view of the apparatus: (a) xenon ion beam; (b) nickel targets; (c) cooling cell; (d) octopole ion guides; (e) first quadrupole mass spectrometer; (f) collision cell; (g) second quadrupole mass spectrometer; (h) ion conversion dynode; (i) secondary electron multiplier.

The spread of the translational energy of a parent cluster ion was determined to be about 4 eV in the laboratory frame by applying a retarding voltage to the octopole ion guide, which is enclosed by the collision cell. This energy spread gives rise to the uncertainty of ±0.2 eV in a collision between Ni_6^+ and a benzene molecule in the center-of-mass frame.

The total reaction cross section, σ_r, is expressed as

$$\sigma_r = \frac{k_B T}{Pl} \ln \frac{I_r + \sum I_p}{I_r} \quad (1)$$

where I_r and $\sum I_p$ represent the intensity of nonreacting parent

* To whom correspondence should be addressed. E-mail: kondow@utsc.s.u-tokyo.ac.jp.
† Genesis Research Institute, Inc.
‡ Toyota Technological Institute.

10.1021/jp014210p CCC: $22.00
Published on Web 04/11/2002

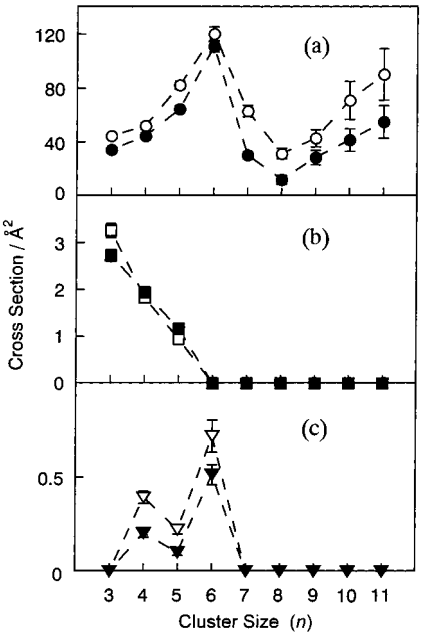

Figure 2. Reaction cross sections for the production of (a) $Ni_n^+(C_6H_6)$, (b) $Ni_{n-1}^+(C_6H_6)$, and (c) $Ni_n^+(C_4H_4)$ at the collision energy of 0.15 eV as a function of the cluster size. The internal temperature is 300 K for the solid symbols and 77 K for the open symbols.

ions and the sum of the intensities of the product ions, respectively, P and T are the pressure and the temperature of benzene gas, respectively, l is the effective path length of the collision region, and k_B is the Boltzmann constant. The partial cross section, σ_p, for the formation of a given product ion was evaluated as

$$\sigma_p = \sigma_r \frac{I_p}{\sum I_p} \tag{2}$$

where $I_p/\sum I_p$ represents the branching ratio of each product ion.

3. Results

The mass spectra of the product ions, $Ni_n^+(C_6H_6)$, $Ni_{n-1}^+(C_6H_6)$, and $Ni_n^+(C_4H_4)$, indicate that the following reaction processes take place:

$$Ni_n^+ + C_6H_6 \rightarrow Ni_n^+(C_6H_6) \tag{3}$$

$$Ni_n^+ + C_6H_6 \rightarrow Ni_{n-1}^+(C_6H_6) + Ni \tag{4}$$

$$Ni_n^+ + C_6H_6 \rightarrow Ni_n^+(C_4H_4) + C_2H_2 \tag{5}$$

Figure 2 shows the cross sections for the three different reaction processes as a function of the cluster size, n, at the collision energy of 0.15 eV in the center-of-mass frame. The cross section for the production of $Ni_n^+(C_6H_6)$ reaches the maximum at the cluster size of 6, that for the production of $Ni_{n-1}^+(C_6H_6)$ is sizable in the size range of 3−5, and that for the production of $Ni_n^+(C_4H_4)$ is measurable only at the sizes of 4−6. Figure 3 shows the total reaction cross section (production of all of the product ions) for the collision of Ni_4^+ with C_6H_6 as a function of the collision energy. The solid and the open circles show the cross sections for the parent cluster ions having the temperatures of 300 and 77 K, respectively. The solid and the broken curves are the calculations given in section 4.3.

4. Discussion

4.1. Reaction Scheme. On the analogy of the $Ni_n^+-CH_3OH$ reaction,[9] the reaction scheme is postulated as follows:

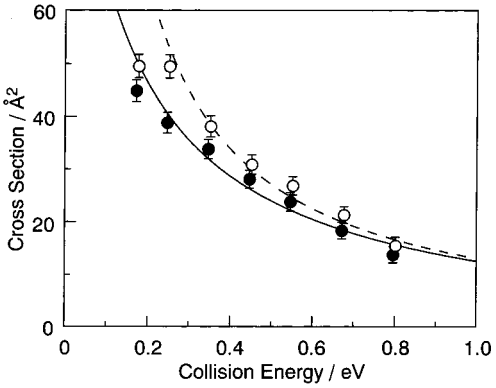

Figure 3. Total reaction cross sections for Ni_4^+ as a function of the collision energy. The solid and open circles exhibit the cross sections at the internal temperature of 300 and 77 K, respectively. The solid and broken lines show the calculated cross sections at the internal temperature of 300 and 77 K, respectively (see text).

$$Ni_n^+ + C_6H_6 \rightarrow [Ni_n^+\cdots(C_6H_6)] \quad \text{(physisorption)} \tag{6}$$

$$[Ni_n^+\cdots(C_6H_6)] \rightarrow [Ni_n^+(C_6H_6)]^\dagger \quad \text{(precursor formation)} \tag{7}$$

$$[Ni_n^+(C_6H_6)]^\dagger \rightarrow Ni_n^+(C_6H_6) \quad \text{(chemisorption)} \tag{8}$$

$$[Ni_n^+(C_6H_6)]^\dagger \rightarrow Ni_{n-1}^+(C_6H_6) + Ni \quad \text{(Ni release)} \tag{9}$$

$$[Ni_n^+(C_6H_6)]^\dagger \rightarrow Ni_n^+(C_4H_4) + C_2H_2 \quad (C_2H_2 \text{ release}) \tag{10}$$

Figure 4 shows a schematic reaction potential related to the reaction process for the C_2H_2 release. A benzene molecule is weakly captured by a nickel cluster ion (physisorption) and converted into a precursor, $[Ni_n^+(C_6H_6)]^\dagger$, from which the product ions are generated.

4.2. Physisorption. In the collision of C_6H_6 with Ni_n^+, C_6H_6 is trapped at first in a weak potential well built by a charge-induced dipole interaction between C_6H_6 and Ni_n^+. The cross section of the trapping, defined as "physisorption", is given by the Langevin cross section, σ_L,

$$\sigma_L = \pi\left(\frac{2\alpha}{E_{col}}\right)^{1/2} \tag{11}$$

where α is the polarizability of C_6H_6 (10.32 Å^3)[13] and E_{col} is the collision energy in the center-of-mass frame.[14] Actually, the largest cross section obtained (chemisorption on Ni_6^+) agrees with the Langevin cross section and turns out to be the upper limit of the physisorption cross section. Note that the Langevin cross section is independent of the cluster size, n.

4.3. Chemisorption. As shown in Figure 4, a physisorbed C_6H_6 is either desorbed or chemisorbed with the rate constants of k_1 and k_2, respectively. The physisorbed C_6H_6 is not detected because its lifetime is too short to arrive at the detector. All of the product ions, $Ni_n^+(C_6H_6)$, $Ni_{n-1}^+(C_6H_6)$, and $Ni_n^+(C_4H_4)$, observed are produced via the precursor, $[Ni_n^+(C_6H_6)]^\dagger$. The cross section, σ_r, for the production of all of the product ions observed is expressed in terms of the Langevin cross section, σ_L, as

$$\frac{\sigma_r}{\sigma_L} = \frac{k_2}{k_1 + k_2} + \frac{k_1}{k_1 + k_2}\exp\{-(k_1 + k_2)t\} \tag{12}$$

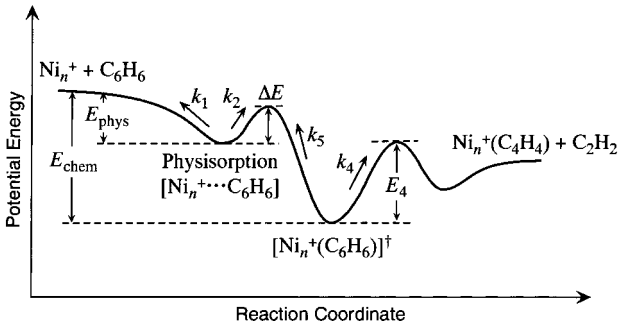

Figure 4. Schematic drawing of the potential energy surface along the reaction coordinate for the production of $Ni_n^+(C_4H_4)$ (see text for the definition of the energy barrier, ΔE, and the rate constants).

where the reaction time, t, is given by the flight time from the collision cell to the second quadrupole mass spectrometer. The cross section, σ_r, is defined as "total reaction cross section".

The rate constants are evaluated by Rice−Ramsperger−Kassel (RRK) theory, which is simpler than Rice−Ramsperger−Kassel−Marcus (RRKM) theory and does not necessitate an insight of the accurate vibrational frequencies. In RRK theory,[15,16] k_1 and k_2 are given by

$$k_1 = A_1\left(\frac{E_{vib} + E_{col}}{E_{vib} + E_{col} + E_{phys}}\right)^{N-1} \quad (13)$$

$$k_2 = A_2\left(\frac{E_{vib} + E_{col} + E_{phys} - \Delta E}{E_{vib} + E_{col} + E_{phys}}\right)^{N-1} \quad (14)$$

where E_{vib}, E_{col}, E_{phys}, and ΔE represent the vibrational energy of the parent cluster ion, the collision energy, the physisorption energy of C_6H_6 on Ni_n^+, and the energy barrier from the physisorbed to the chemisorbed state, respectively (see Figure 4). The total internal energy of the physisorbed intermediate is given as $E_{vib} + E_{col} + E_{phys}$. The coefficients, A_1 and A_2, are the frequency prefactors related to the $Ni_n^+-C_6H_6$ dissociation and the chemisorption from the physisorption, respectively, and N is the total number of the vibrational modes of $Ni_n^+(C_6H_6)$ less the internal modes of C_6H_6 ($N = \{3(n + 12) - 6\} - \{3 \times 12 - 6\} = 3n$).

Using eqs 12−14, one can calculate the dependence of the total reaction cross section on the collision energy at a given internal temperature. Figure 3 shows the total reaction cross section for the Ni_4^+ reaction as a function of the collision energy (see section 3). The calculated cross sections for the temperatures of 300 and 77 K are plotted as the solid and broken curves, respectively; the curves are obtained from eqs 12−14 leaving $\Delta E/E_{phys}$ and A_1/A_2 as the fitting parameters. The best-fit values of $\Delta E/E_{phys}$ and A_1/A_2 are obtained to be 0.87 and 6.50, respectively. The total reaction cross sections measured agree well with the theoretical cross sections.

Figure 5 shows the size dependence of $\Delta E/E_{phys}$ thus obtained with A_1/A_2 of 6.50. It is evident that $\Delta E/E_{phys}$ shows anticorrelation with the total reaction cross section, σ_r (see Figures 2 and 5); for instance, $\Delta E/E_{phys}$ exhibits the minimum at $n = 6$, whereas σ_r exhibits the maximum. This anticorrelation implies that the chemisorption proceeds most efficiently at $n = 6$ because the lowest energy barrier is attained at this size.

4.4. Ni Release. It is considered that $Ni_{n-1}^+(C_6H_6)$ is generated by unimolecular dissociation of the precursor, $[Ni_n^+(C_6H_6)]^\dagger$. When one vibrational mode of the precursor related to the $Ni_{n-1}^+(C_6H_6)-Ni$ bond rupture happens to gain an energy larger than the dissociation energy, E_{dis}, of the bond, the

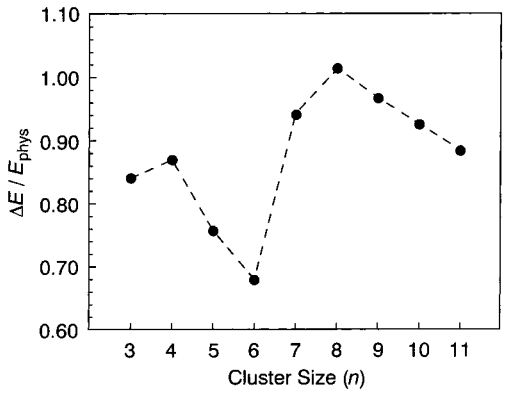

Figure 5. The ratio $\Delta E/E_{phys}$ plotted against the cluster size (see text for the definition of ΔE and E_{phys}).

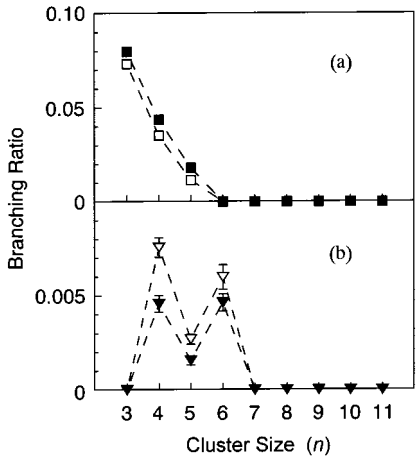

Figure 6. Branching ratio (a) $[Ni_{n-1}^+(C_6H_6)]/[Ni_n^+(C_6H_6)]$ and (b) $[Ni_n^+(C_4H_4)]/[Ni_n^+(C_6H_6)]$ as a function of the cluster size. The solid and open symbols show the data points for the internal temperatures of 300 and 77 K, respectively. The collision energy is fixed at 0.15 eV.

precursor dissociates into $Ni_{n-1}^+(C_6H_6) + Ni$. The branching ratio of the $Ni_{n-1}^+(C_6H_6)$ production with respect to the $Ni_n^+(C_6H_6)$ production is expressed as

$$\frac{[Ni_{n-1}^+(C_6H_6)]}{[Ni_n^+(C_6H_6)]} = \frac{1 - \exp(-k_3 t)}{\exp(-k_3 t)} \quad (15)$$

where k_3 represents the rate constant of the $[Ni_n^+(C_6H_6)]^\dagger$ dissociation with releasing Ni.

Figure 6a shows the branching ratio, $[Ni_{n-1}^+(C_6H_6)]/[Ni_n^+(C_6H_6)]$, at the collision energy of 0.15 eV as a function of the cluster size. The solid and open squares exhibit the cross sections at the internal temperatures of 300 and 77 K, respectively. By using RRK theory, k_3 is given as

$$k_3 = \nu\left(\frac{E_{vib} + E_{col} + E_{chem} - E_{dis}}{E_{vib} + E_{col} + E_{chem}}\right)^{N-1} \quad (16)$$

where E_{vib}, E_{col}, and E_{chem} represent the vibrational energy of the parent cluster ion, the collision energy, and the chemisorption energy of C_6H_6 on Ni_n^+, respectively, and ν is the prefactor related to the vibrational frequency of the $Ni_{n-1}^+(C_6H_6)-Ni$ bond rupture. In this analysis, the prefactor is approximated by the frequency of a Ni−Ni bond of Ni_n^+ and is estimated from the vibrational frequency of a nickel dimer (328 cm^{-1})[17] and the Debye temperature of a nickel crystal by using Jarrold and Bower's method.[18] The dissociation energy, E_{dis}, of the Ni_{n-1}^+-

(C_6H_6)−Ni bond is approximated by the Ni_{n-1}^+−Ni bond dissociation energy of a bare Ni_n^+.[19] By comparison of the measured branching ratio, $[Ni_{n-1}^+(C_6H_6)]/[Ni_n^+(C_6H_6)]$, with the theoretical one calculated by eqs 15 and 16, E_{chem} values are estimated to be 2.4, 2.0, and 2.4 eV for $n = 3$, 4, and 5, respectively. The chemisorption energies of C_6H_6 on Ni_n^+ thus obtained are comparable to the binding energy of C_6H_6 with Ni^+ in the gas phase (2.95 eV)[20] or the chemisorption energy of C_6H_6 on a Ni(100) surface (1.23 eV).[21]

The monotonic decrease of the reaction cross section with the cluster size is explained by RRK theory in such a manner that the energy partitioned to the internal mode related to the reaction decreases with the cluster size, owing to the increase of the number of the vibrational degrees of freedom with the cluster size. No reaction for $n \geq 6$ is explained by the energetics of the reaction as follows: The dissociation energy of Ni_{n-1}^+−Ni is reported to be less than 2.4 eV for $n < 6$ and is more than 2.4 eV for $n \geq 6$.[19] As the cluster size increases, the chemisorption energy of C_6H_6 on Ni_n^+ is expected to decrease approaching to the chemisorption energy of C_6H_6 on a nickel surface. It implies that the internal energy of $[Ni_n^+(C_6H_6)]^\dagger$ is too small to release a Ni atom from it for $n = 6$.

4.5. C_2H_2 Release. Figure 6b shows the branching ratio, $[Ni_n^+(C_4H_4)]/[Ni_n^+(C_6H_6)]$, for the Ni_n^+ reaction at the collision energy of 0.15 eV. The solid and open triangles exhibit the cross sections at the internal temperatures of 300 and 77 K, respectively. Let us consider that $Ni_n^+(C_4H_4)$ is produced by the unimolecular dissociation of $[Ni_n^+(C_6H_6)]^\dagger$ with releasing C_2H_2. The precursor, $[Ni_n^+(C_6H_6)]^\dagger$, undergoes decomposition either into $Ni_n^+(C_4H_4) + C_2H_2$ by surmounting the energy barrier, E_4, or back into C_6H_6 and Ni_n^+. The rate constants of the former and the latter processes are written as k_4 and k_5, respectively. Note that the rate constant, k_5, of $[Ni_n^+(C_6H_6)]^\dagger$ dissociation into Ni_n^+ and C_6H_6 is considered to be small. Therefore, the back reaction into Ni_n^+ and C_6H_6 is disregarded in the argument of the chemisorption or $Ni_{n-1}^+(C_6H_6)$ formation discussed above.

By using k_4 and k_5, the branching ratio, $[Ni_n^+(C_4H_4)]/[Ni_n^+(C_6H_6)]$, is expressed as

$$\frac{[Ni_n^+(C_4H_4)]}{[Ni_n^+(C_6H_6)]} = \frac{k_4}{k_4 + k_5} \frac{1 - \exp\{-(k_4 + k_5)t\}}{\exp\{-(k_4 + k_5)t\}} \quad (17)$$

The rate constants, k_4 and k_5, are given by RRK theory. Throughout the calculation, E_{phys} is approximated to be 0.4 eV by the energy of the charge-induced dipole interaction, while E_{chem} is estimated in section 4.4. The total number of the vibrational modes of $[Ni_n^+(C_6H_6)]^\dagger$ is regarded as N for the decomposition of $[Ni_n^+(C_6H_6)]^\dagger$ into $Ni_n^+(C_4H_4) + C_2H_2$, because the internal modes of C_6H_6 should contribute to the decomposition of C_6H_6 on Ni_n^+. The energy barrier, E_4, is obtained to be ~1 eV by the comparison of the calculated branching ratio (see eq 17) with the experimental one. In conclusion, the C_2H_2 release occurs only at the cluster sizes of 4−6, probably because the energy barrier, E_4, is low particularly in this size range.

Acknowledgment. The authors are grateful to Prof. L. H. Wöste and Prof. T. Leisner for their assistance in designing the metal ion source. Thanks are also due to Prof. S. Tanemura and Dr. J. Murakami for valuable information on the operation of the metal ion source. This work is supported by Special Cluster Research Project of Genesis Research Institute, Inc.

References and Notes

(1) Che, M.; Bennett, C. O. *Adv. Catal.* **1989**, *36*, 55.
(2) Grimley, T. B. In *Electronic Structure and Reactivity of Metal Surfaces*; Derouane, E. G., Lucas, A. A., Eds; Plenum Press: New York, 1976; pp 35−43.
(3) Fayet, P.; McGlinchey, M. J.; Wöste, L. H. *J. Am. Chem. Soc.* **1987**, *109*, 1733.
(4) Vajda, S.; Wolf, S.; Leisner, T.; Busolt, U.; Wöste, L. H. *J. Chem. Phys.* **1997**, *107*, 3492.
(5) Irion, M. P.; Schnabel, P.; Selinger, A. *Ber. Bunsen-Ges. Phys. Chem.* **1990**, *94*, 1291.
(6) Irion, M. P.; Schnabel, P. *Ber. Bunsen-Ges. Phys. Chem.* **1992**, *96*, 1091.
(7) Vann, W. D.; Castleman, A. W., Jr. *J. Phys. Chem. A* **1999**, *103*, 847.
(8) Vann, W. D.; Bell, R. C.; Castleman, A. W., Jr. *J. Phys. Chem. A* **1999**, *103*, 10846.
(9) Ichihashi, M.; Hanmura, T.; Yadav, R. T.; Kondow, T. *J. Phys. Chem. A* **2000**, *104*, 11885.
(10) Ichihashi, M.; Hirokawa, J.; Nonose, S.; Nagata, T.; Kondow, T. *Chem. Phys. Lett.* **1993**, *204*, 219.
(11) Ichihashi, M.; Nonose, S.; Nagata, T.; Kondow, T. *J. Chem. Phys.* **1994**, *100*, 6458.
(12) Hirokawa, J.; Ichihashi, M.; Nonose, S.; Tahara, T.; Nagata, T.; Kondow, T. *J. Chem. Phys.* **1994**, *101*, 6625.
(13) Lide, D. R. *CRC Handbook of Chemistry and Physics*, 78th ed.; CRC Press: Boca Raton, FL, 1997.
(14) Levine, R. D.; Bernstein, R. B. *Molecular Reaction Dynamics*; Oxford University Press: Oxford, U.K., 1974.
(15) Kassel, L. S. *J. Phys. Chem.* **1928**, *32*, 225.
(16) Draves, J. A.; Luthey-Schulten, Z.; Liu, W.-L.; Lisy, J. M. *J. Chem. Phys.* **1990**, *93*, 4589.
(17) Morse, M. D. *Chem. Rev.* **1986**, *86*, 1049.
(18) Jarrold, M. F.; Bower, J. E. *J. Chem. Phys.* **1987**, *87*, 5728.
(19) Lian, L.; Su, C.-X.; Armentrout, P. B. *J. Chem. Phys.* **1992**, *96*, 7542.
(20) Hettich, R. I.; Freiser, B. S. *J. Am. Chem. Soc.* **1987**, *109*, 3537.
(21) Myers, A. K.; Schoofs, G. R.; Benziger, J. B. *J. Phys. Chem.* **1987**, *91*, 2230.